A Cyber-Physical System Perspective on Large Signal Stability of DC Microgrid Clusters

Sucheng LIU, Chao FANG, Xuefeng HUANG, Qianjin ZHANG, Wei FANG, and Xiaodong LIU

***Abstract*—DC microgrid cluster (DCMGC) is a dynamic network formed by connecting a group of geographically neighboring DC microgrids (DCMGs) through tie-lines. Each DCMG collaborates with other DCMGs to achieve maximum economic benefits through flexible power flow management within the DCMG and at the system level. Therefore, DCMGCs require communication, computing, and control to manage the power flow. As a result, the DCMGCs are naturally represented as cyber-physical systems (CPSs). However, DCMGCs are of high penetration of distributed energy resources, which creates significant randomness at both resource and load sides. Consequently, these systems will experience large disturbances leading to serious stability problems like high oscillations or even collapse. In this paper, Takagi-Sugeno (T-S) modeling is utilized to reduce the large signal Lyapunov stability of DCMGs to a series of linear matrix inequalities (LMIs). The impact of key circuit parameters, control parameters, communication delay, and cyber-attacks on the large signal stability of DCMGCs is revealed, and the region of attraction (ROA) of the network is estimated as well. Finally, the large signal stability analysis is verified by experimental results. The findings of this work will be instrumental in developing more effective control strategies to enhance the stability and reliability of DCMGCs.**

***Index Terms*—Cyber-physical system, DC microgrid cluster, large signal stability, Takagi-Sugeno (T-S) modeling.**

I. Introduction

OVER the last few decades, microgrids have been proven to be an effective means of utilizing distributed energy resources (DERs). While AC microgrids (ACMGs) were proposed two decades ago, DC microgrids (DCMGs) were intensively researched in recent years. DCMGs have more appealing features, such as a simpler structure, higher efficiency, and lower cost, and are becoming the top priority in implementing DER-based power generation systems with more sources and loads of DC nature locally [1], [2]. Following the success of DCMGs, it is natural to consider interconnecting multiple geographically neighboring DCMGs as a networked microgrid (NMG) or a cluster. Such interconnected topologies of DCMGs can increase resilience, reliability, and economic benefits to a new level. However, the advent of DCMG clusters (DCMGCs) presents many unprecedented challenges due to their more complex network structures.

The management of complex DCMGCs involves a hierarchical control system consisting of three levels: primary, secondary, and tertiary [3]. Multiple control objectives can be assigned to each level to facilitate the decoupled design of the systems in a simplified manner. At the bottom level [4]–[7], the primary and secondary controls focus on current sharing and voltage restoration within each DCMG, while the tertiary control at the top manages power flow among interconnected DCMGs in the DCMGC [8]–[11]. Effective management of power flow necessitates communication, computing, and control, rendering DCMGCs typical cyber-physical systems (CPSs). Additionally, DCMGCs have a high penetration of DERS, resulting in significant randomness on both the resource and load sides. Furthermore, the emergence of controlled electronic loads with constant power load (CPL) characteristics poses a significant threat to system stability. Consequently, these systems will experience large disturbances leading to serious stability problems, such as high oscillations or even collapse.

In principle, the stabilities of DCMGCs can be classified as either small signal or large signal depending on the magnitude of disturbances. Small signal stability allows for the use of linear systems tools, such as the Roth-Hurwitz criterion, root locus, and Nyquist criterion, which are based on linearized models around equilibrium points of nonlinear dynamic systems. On the other hand, large signal stability preserves the nonlinear characteristics of the systems, and requires the use of advanced tools, such as Takagi-Sugeno (T-S) modeling [12], Lyapunov functions, mixed potential functions [13], and the reverse trajectory principle [14]. Currently, there is a wealth of research on stabilities of both small and large signal at the single DCMG scale, with a greater emphasis on small signal stability.

The pioneering analysis on large signal stability of a distributed power system with CPL was carried out in [15] where the mixed potential function is used as the stability criterion of Lyapunov function stability analysis. Recently, the large signal stability caused by CPL has also been widely studied in DCMG [16]. Based on the mixed potential

Manuscript received August 6, 2023; revised November 23, 2023; accepted December 18, 2023. Date of publication March 30, 2024; date of current version January 2, 2024. This work was supported by the National Natural Science Foundation of China under grant 52277169 and in part by the Key Laboratory of Fujian Universities for New Energy Equipment Testing under grant XNY202106, and Natural Science Research Project of Anhui Educational Committee under grant 2022AH050326. *(Corresponding author: Sucheng Liu.)*

All authors are with the Anhui Provincial Key Laboratory of Power Electronics and Motion Control, Anhui University of Technology, Ma'anshan, 243032, China (e-mail: liusucheng@ahut.edu.cn; fangchao2050@163.com; huangxuefeng1117@163.com; zqj1214@ahut.edu.cn; fwei2k@163.com; liuxiaodong@ahut.edu.cn).

Digital Object Identifier 10.24295/CPSSTPEA.2023.00050

criterion, the influence of CPL and energy storage system is considered, and the relationship between system parameters and stability is quantitatively analyzed [17]. The large signal stability sufficient criterion of DCMG with distributed control is proposed by mixed potential theory in [18]. In [19], the conservatism of the mixed potential theory in large signal stability criterion of the DCMG is improved by optimizing the modeling of CPL converter, but the stable operation parameters analysis of the DCMG are absent. In [20], the local stability of each equilibrium point is discussed in the large signal global stability analysis of the system, and the ROA of the microgrid system is estimated to investigate the local stability of each equilibrium point. Some key points of mixed potential theory are emphasized and the large signal stability analysis of DC distribution network with CPL is analyzed. Besides, the stability of each equilibrium is analyzed, and all the low-voltage equilibrium is proved to be unstable and the analytical stability condition for the high-voltage equilibrium is provided [21]. The equivalent model of droop control DCMG is established from the system level to solve the problem of large signal stability analysis of DCMG [22]–[27]. In [28], the large signal stability theory of system with shunt active damper is derived. However, the system only carries out a simple study on one CPL, and it is necessary to analyze a more complex system. The stability of large-signal disturbances in DCMG with multiple CPLs is studied, by using the T-S fuzzy model [29]. In [30], a novel decentralized composite controller is proposed to serve as a large signal stabilizer for a DCMG system, escalating the MG flexibility and reliability to a large measure. All these works promote the advances of large signal stability of single DCMG in stand-alone.

However, research on stability at the DCMGC scale is still relatively scarce, particularly in the context of large signal stability [31], [32]. The large signal stability of DCMGCs with ZIP load was firstly explored in [32] where the T-S fuzzy multi-modeling approach is utilized to reduce the large signal Lyapunov stability of the systems to a series of linear matrix inequalities (LMIs). Nevertheless, only the main circuit are considered as the case of study, and the impact of control and communication on the large signal stability of the DCMGCs is absent.

Indeed, the existing studies have verified the key playing roles of control and communications in influencing the stability of CPSs, especially in MG systems. The most influencing factors that have been identified are the communication delay and cyber-attacks. In [33], the time-delay in hierarchical control of DCMGs in stand-alone is considered, and the stability of the hybrid energy storage system for maintaining the upper bound of maximum delay is determined. A method of establishing MG small signal model with the secondary voltage control is proposed, and then the influence of communication delay on system stability is analyzed [34], [35]. The multi-delay small-signal stability analysis of DCMGCs with distributed hierarchical control architecture is studied in [36]. On the other hand, various cyber-attacks such as malicious cyber-attacks like false data injection attack (FDIA), denial of service (DoS) attack, spoofing attack, replay attack, have also been paid intensive attention since they will jeopardize the stable operation of MGs. In [37], the influence of intermittent denial of service (IDoS) attack on the security of cyber-physical MGs is studied, and the stability of cyber-physical microgrid under IDoS attack is analyzed. In [38], the stability analysis of a class of CPS under DoS attack is studied, and by transforming the stability analysis of the system under DoS into the stability analysis of the auxiliary system, the online stability monitoring strategy is developed. A novel adaptive stabilization method is presented to eliminate the instability of DCMG system caused by stealthy cyber-attacks [39]. An cyber-resilient distributed controller design with guaranteed stability is proposed for cooperative DCMGs [40]. In short, the communication network has an important influence on the stability of DCMGs and DCMGCs. Most important of all, the impact of control and communication on the large signal stability of the DCMGCs remains an open topic for research.

Hence, the absence of impact of control and communication on large signal stability of DCMGCs motivates the work and necessitates the perspective of CPS into this problem. The main contributions are twofold:

(1) The large signal stability of the distributed hierarchical control of DCMGCs is investigated from the perspective of a typical CPS, and the adopted T-S modeling approach facilitates the computation of the Lyapunov functions that guarantee the sufficient conditions of large signal stability of the systems.

(2) In addition to the main circuit parameters, the influences of the hierarchical controller parameters, the communication delay, and the cyber-attacks (FDIAs) on the large signal stability of DCMGCs are revealed in terms of the predicted stability region, viz., the region of attraction (ROA), and the key findings can be utilized for large signal stabilization of DCMGCs.

The rest of the paper is organized as follows: Section II performs large signal modeling of the DCMGCs with distributed hierarchical control. Section III derives the large signal stability criteria that consider communication delay and cyber-attack. Section IV presents the large signal stability analysis of the DCMGC, and the evolution of the ROA with the influencing factors, i.e., main circuit, hierarchical controller parameters, time-delay, and FDIAs, are all revealed. Section V validates the analysis by experimental results. Conclusions of the work are finally drawn in Section VI.

II. Reduced Large Signal Modeling of the DCMGC

The DCMGC as a CPS is shown in Fig. 1 where not only the physical layer (power stage) is illustrated but the communication network and the control block diagram are given as well. In the physical layer, the DCMGC consists of n DCMGs that are interconnected through tie-lines. Each DCMG is composed of three basic components, i.e., energy storage system, renewable energy resource, and load, and here the battery energy storage systems (BESS), the photovoltaic (PV) system, and the CPL are highlighted for example.

In the cyber layer, the communication graph is described, and

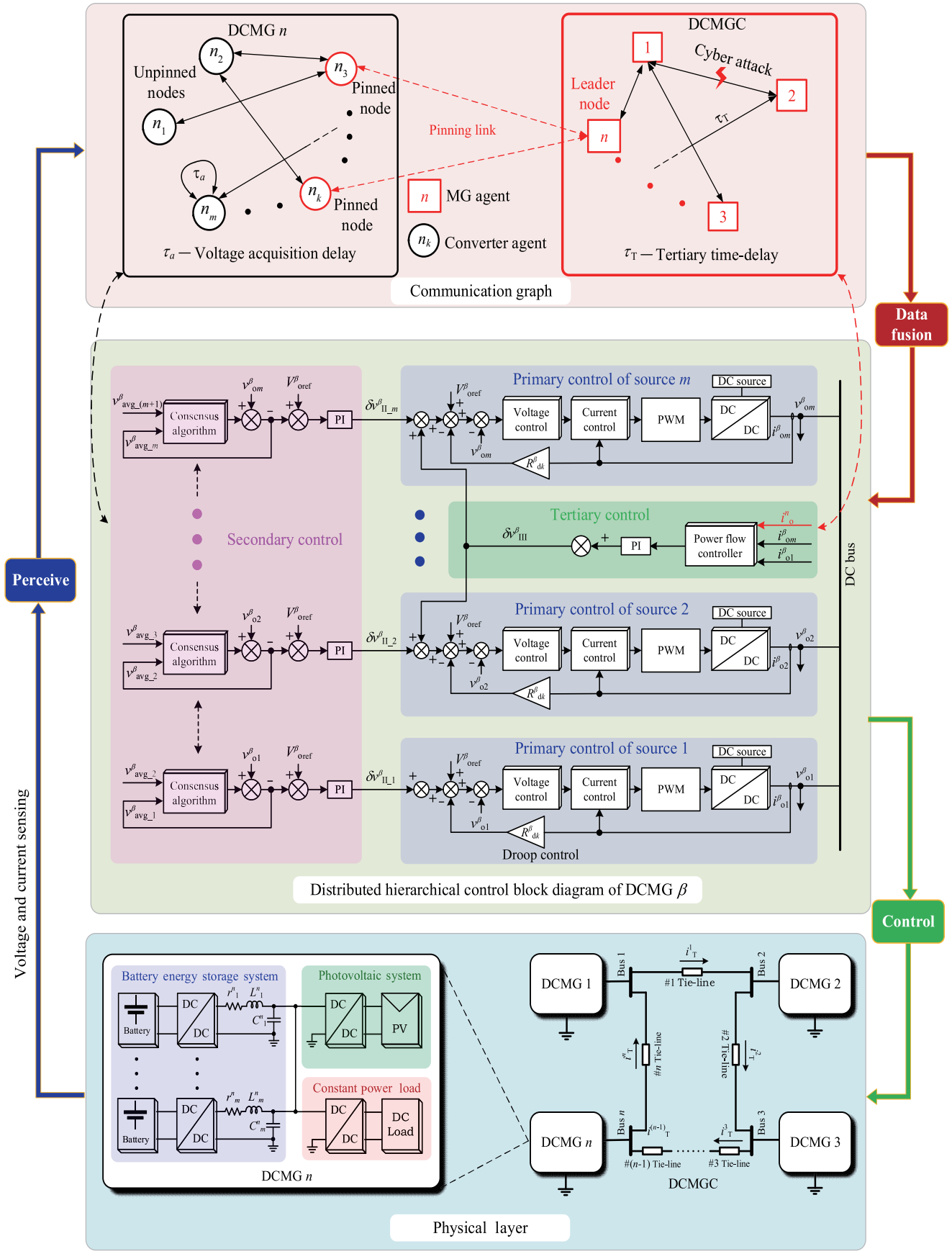

Fig. 1. The DCMGC as a cyber-physical system (CPS).

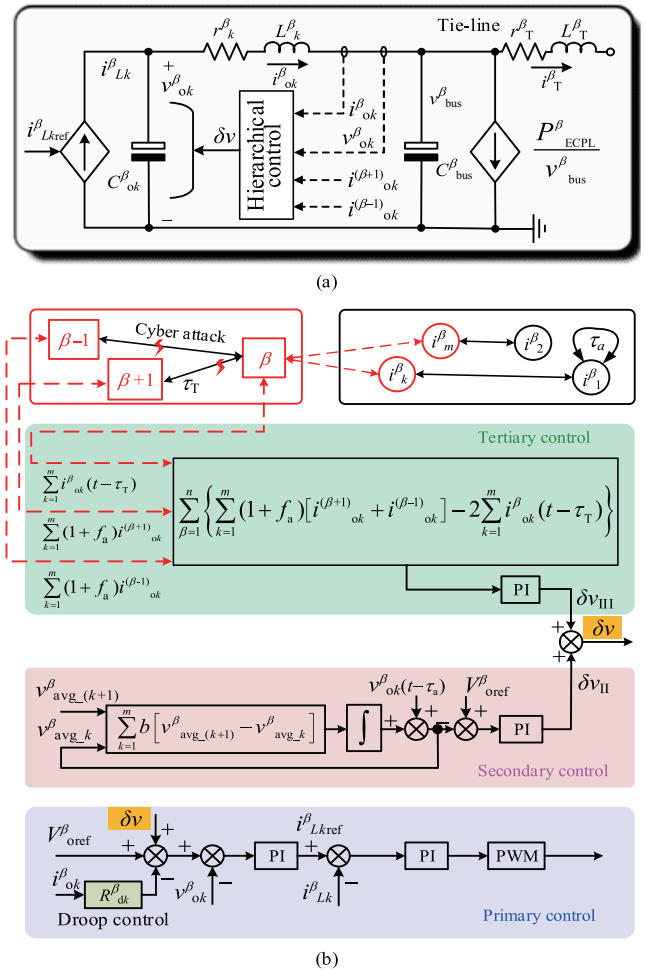

Fig. 2. Modeling of single DCMG. (a) Reduced large signal model of the DCMG β. (b) Block diagram of the distributed hierarchical control with communications.

the global communication of the DCMGC for the information exchange between MGs and the local communication of each DCMG for that between converter agents are depicted for distributed tertiary control and secondary control respectively. The communication between the global and the local graph is achieved via the pinning link. In addition, the control block diagram of the hierarchical control is illustrated where the primary, the secondary, and the tertiary control are all given.

To facilitate large signal stability analysis of the complex DCMGC as the CPS, it is necessary to reduce the model of every single DCMG, and thus render the derived model manageable. Fortunately, hierarchical control provides an effective way to accomplish the model reduction of the DCMGC since the dynamics in the different control levels can be arguably separated by the time-scales.

With the hierarchical control of the DCMGC in Fig. 1, every single DCMG can be approximated by the reduced-order model in large-signal sense [22], [32], [41], and more detailed control block diagram are shown in Fig. 2.

In the dual-loop control of the grid-forming (BESS) converter, the inductor branch is represented by the controlled-current source due to very fast response of the inner current loop that the primary (droop) is readily incorporated by the virtual resistance. Specifically, the primary control including the outer voltage loop and the droop is described as

$$\begin{cases} \delta v = \delta v^{\beta}_{\mathrm{II}\_k} + \delta v^{\beta}_{\mathrm{III}} \\ i^{\beta}_{Lk\mathrm{ref}} = K^{\beta}_{\mathrm{pv}\_k}\left(V^{\beta}_{\mathrm{oref}} + \delta v - i^{\beta}_{ok} R^{\beta}_{dk} - v^{\beta}_{ok}\right) + \\ \qquad K^{\beta}_{\mathrm{iv}\_k}\int\left(V^{\beta}_{\mathrm{oref}} + \delta v - i^{\beta}_{ok} R^{\beta}_{dk} - v^{\beta}_{ok}\right)\mathrm{d}t \end{cases} \tag{1a}$$

Similarly, the secondary control is written as

$$\begin{cases} v^{\beta}_{\mathrm{avg}\_k} = \int\sum b\left[v^{\beta}_{\mathrm{avg}-(k+1)} - v^{\beta}_{\mathrm{avg}-k}\right]\mathrm{d}t + v^{\beta}_{ok}(t-\tau_a) \\ \delta v^{\beta}_{\mathrm{II}\_k} = K^{\beta}_{\mathrm{pII}\_k}\left(V^{\beta}_{\mathrm{oref}} - v^{\beta}_{\mathrm{avg}\_k}\right) + K^{\beta}_{\mathrm{iII}\_k}\int\left(V^{\beta}_{\mathrm{oref}} - v^{\beta}_{\mathrm{avg}\_k}\right)\mathrm{d}t \end{cases} \tag{1b}$$

and the tertiary control is given by

$$\begin{aligned} \delta v^{\beta}_{\mathrm{III}} = K^{\beta}_{\mathrm{pIII}}\sum_{\beta=1}^{n}\left[\sum_{k=1}^{m}(1+f_{\mathrm{a}})i^{(\beta+a)}_{ok} - \sum_{k=1}^{m} i^{\beta}_{ok}(t-\tau_{\mathrm{T}})\right] + \\ K^{\beta}_{\mathrm{iIII}}\int\sum_{\beta=1}^{n}\left[\sum_{k=1}^{m}(1+f_{\mathrm{a}})i^{(\beta+a)}_{ok} - \sum_{k=1}^{m} i^{\beta}_{ok}(t-\tau_{\mathrm{T}})\right]\mathrm{d}t \end{aligned} \tag{1c}$$

where $\delta v^{\beta}_{\mathrm{II}\_k}$ and $\delta v^{\beta}_{\mathrm{III}}$ are the regulation terms due to secondary and tertiary control of DCMG β, respectively; $V^{\beta}_{\mathrm{oref}}$, R^{β}_{dk}, i^{β}_{ok}, v^{β}_{ok} are reference voltage, droop coefficients , output current and output voltage of converter k in DCMG β respectively; $K^{\beta}_{\mathrm{pv}\_k}$, $K^{\beta}_{\mathrm{iv}\_k}$, $K^{\beta}_{\mathrm{pII}\_k}$, $K^{\beta}_{\mathrm{iII}\_k}$, $K^{\beta}_{\mathrm{pIII}}$ and $K^{\beta}_{\mathrm{iIII}}$ are primary control proportional gain, primary control integral gain, secondary control proportional gain, secondary control integral gain, tertiary control proportional gain and tertiary control integral gain, respectively; $v^{\beta}_{\mathrm{avg}\_(k+1)}$ and $v^{\beta}_{\mathrm{avg}\_k}$ denote average output voltages of the adjacent converters to converter k in DCMG β by the consensus algorithm, respectively; f_{a}, τ_{a} and τ_{T} are the FDIA coefficient, voltage acquisition delay and tertiary communication delay, respectively.

To analyze the influence of hierarchical control on the DCMGC, a set of new state variables are introduced by setting the integral term of the control loop that can be described as

$$\begin{cases} \omega^{\beta}_{\mathrm{III}} = \int\sum_{\beta=1}^{n}\left[\sum_{k=1}^{m}(1+f_{\mathrm{a}})i^{(\beta+a)}_{ok} - \sum_{k=1}^{m} i^{\beta}_{ok}(t-\tau_{\mathrm{T}})\right]\mathrm{d}t \\ \omega^{\beta}_{\mathrm{avg}\_k} = \int\sum b\left[v^{\beta}_{\mathrm{avg}\_(k+1)} - v^{\beta}_{\mathrm{avg}\_k}\right]\mathrm{d}t \\ \omega^{\beta}_{\mathrm{II}\_k} = \int\left(V^{\beta}_{\mathrm{oref}} - v^{\beta}_{\mathrm{avg}\_k}\right)\mathrm{d}t \\ \omega^{\beta}_{\mathrm{I}\_k} = \int\left[V^{\beta}_{\mathrm{oref}} + \delta v - i^{\beta}_{ok} R^{\beta}_{dk} - v^{\beta}_{ok}(t-\tau_{\mathrm{a}})\right]\mathrm{d}t \end{cases} \tag{2}$$

where $\omega^{\beta}_{\mathrm{III}}$, $\omega^{\beta}_{\mathrm{II}\_k}$, $\omega^{\beta}_{\mathrm{I}\_k}$ and $\omega^{\beta}_{\mathrm{avg}\_k}$ are the tertiary control state variable, secondary control state variable of converter k, primary control state variable, dynamic consensus algorithm state variable of converter k of DCMG β, respectively.

Given the large signal model of single DCMG in Fig. 2, and meanwhile to incorporate the tie-lines with interconnection of n MGs in the DCMGC, the overall large signal model of the

DCMGC can be derived as

$$
\begin{cases}
\left.\begin{aligned}
&\frac{\mathrm{d}\omega^1_{\mathrm{III}}}{\mathrm{d}t}=\sum_{k=1}^{m}\left[(1+f_{\mathrm{a}})(i^n_{ok}+i^2_{ok})-2i^1_{ok}(t-\tau_{\mathrm{T}})\right]\Big\}\text{Tertiary control}\\
&\frac{\mathrm{d}\omega^1_{\mathrm{II}\_k}}{\mathrm{d}t}=V^1_{\mathrm{oref}}-\omega^1_{\mathrm{avg}\_k}-v^1_{ok}(t-\tau_{\mathrm{a}})\Big\}\text{Secondary control}\\
&\frac{\mathrm{d}\omega^1_{\mathrm{I}\_k}}{\mathrm{d}t}=V^1_{\mathrm{oref}}+\delta v-i^1_{ok}R^1_{dk}-v^1_{ok}(t-\tau_{\mathrm{a}})\Big\}\text{Primary control}\\
&C^1_{ok}\frac{\mathrm{d}v^1_{ok}}{\mathrm{d}t}=i^1_{Lk}-i^1_{ok}\\
&L^1_k\frac{\mathrm{d}i^1_{ok}}{\mathrm{d}t}=v^1_{ok}(t-\tau_{\mathrm{a}})-i^1_{ok}r^1_k-v^1_{\mathrm{bus}}\Big\}\text{Power stage}\\
&C^1_{\mathrm{bus}}\frac{\mathrm{d}v^1_{\mathrm{bus}}}{\mathrm{d}t}=\sum_{k=1}^{m}i^1_{ok}-\frac{P^1_{\mathrm{ECPL}}}{v^1_{\mathrm{bus}}}-i^1_{\mathrm{T}}
\end{aligned}\right\}\text{DCMG 1}\\
\quad\vdots\\
\left.\begin{aligned}
&\frac{\mathrm{d}\omega^n_{\mathrm{III}}}{\mathrm{d}t}=\sum_{k=1}^{m}\left\{(1+f_{\mathrm{a}})[i^{(n+1)}_{ok}+i^{(n-1)}_{ok}]-2i^n_{ok}(t-\tau_{\mathrm{T}})\right\}\\
&\frac{\mathrm{d}\omega^n_{\mathrm{II}\_k}}{\mathrm{d}t}=V^n_{\mathrm{oref}}-\omega^n_{\mathrm{avg}\_k}-v^n_{ok}(t-\tau_{\mathrm{a}})\\
&\frac{\mathrm{d}\omega^n_{\mathrm{I}\_k}}{\mathrm{d}t}=V^n_{\mathrm{oref}}+\delta v-i^n_{ok}R^n_{dk}-v^n_{ok}(t-\tau_{\mathrm{a}})\\
&C^n_{ok}\frac{\mathrm{d}v^n_{ok}}{\mathrm{d}t}=i^n_{Lk}-i^n_{ok}\\
&L^n_k\frac{\mathrm{d}i^n_{ok}}{\mathrm{d}t}=v^n_{ok}(t-\tau_a)-i^n_{ok}r^n_k-v^n_{\mathrm{bus}}\\
&C^n_{\mathrm{bus}}\frac{\mathrm{d}v^n_{\mathrm{bus}}}{\mathrm{d}t}=\sum_{k=1}^{m}i^n_{ok}-\frac{P^n_{\mathrm{ECPL}}}{v^n_{\mathrm{bus}}}-i^n_{\mathrm{T}}
\end{aligned}\right\}\text{DCMG }n\\
\left.\begin{aligned}
&L^1_{\mathrm{T}}\frac{\mathrm{d}i^1_{\mathrm{T}}}{\mathrm{d}t}=v^1_{\mathrm{bus}}-i^1_{\mathrm{T}}r^1_{\mathrm{T}}-v^2_{\mathrm{bus}}\\
&\quad\vdots\\
&L^n_{\mathrm{T}}\frac{\mathrm{d}i^n_{\mathrm{T}}}{\mathrm{d}t}=v^n_{\mathrm{bus}}-i^n_{\mathrm{T}}r^n_{\mathrm{T}}-v^1_{\mathrm{bus}}
\end{aligned}\right\}\text{Tie-lines}
\end{cases}
\tag{3}
$$

where $i^{(\beta+1)}_{\mathrm{ok}}$ and $i^{(\beta-1)}_{\mathrm{ok}}$ represent the output current of BESS of the adjacent converters k in DCMG β, respectively; C^{β}_{ok}, L^{β}_k, r^{β}_k, C^{β}_{bus}, $P^{\beta}_{\mathrm{ECPL}}$, r^{β}_{T} and L^{β}_{T} are output capacitance, line inductance, line resistance of converter k, bus capacitance, equivalent CPL, tie-line resistance and tie-line inductance of DCMG β, respectively; v^{β}_{bus} and i^{β}_{T} are bus voltage and tie-line current of DCMG β, respectively.

The model in (3) presents two significant features: 1) The comprehensive model is with multiple nonlinearities, e.g., CPL, time-delay, etc., which necessitates nonlinear systems tools to analyze the large signal behavior of the DCMGC; 2) The model is of higher-order system, and the order will be $7\times n$ or $7\times n-1$, where n denotes the number of MGs. For example, (3) can be over 20th order with three MGs interconnected.

In the next section, the characteristics of the nonlinearity and high-order of the large signal model of the DCMGC will be tackled by the T-S fuzzy modeling approach, which facilitates the derivation of the large signal stability criteria.

III. Large Signal Stability Criteria of the DCMGC

A. T-S Fuzzy Modeling of the DCMGC

For convenience, the model in (3) can be rewritten as the compact form of

$$\dot{\boldsymbol{x}}(t)=f\left[\boldsymbol{x}(t),\boldsymbol{u}(t)\right] \tag{4}$$

where $\boldsymbol{x}(t)=[\omega^1_{\mathrm{III}}, \omega^1_{\mathrm{II}\_k}, \omega^1_{\mathrm{I}\_k}, v^1_{ok}, i^1_{ok}, v^1_{\mathrm{bus}}, \ldots, \omega^n_{\mathrm{III}}, \omega^n_{\mathrm{II}\_k}, \omega^n_{\mathrm{I}\_k}, v^n_{ok}, i^n_{ok}, v^n_{\mathrm{bus}}, i^1_{\mathrm{T}}, \ldots, i^n_{\mathrm{T}}]^{\mathrm{T}}$, and $\boldsymbol{u}(t)=[0, V^1_{\mathrm{oref}}, \omega^1_{\mathrm{avg}\_k}, 0, 0, 0, \ldots, 0, V^n_{\mathrm{oref}}, \omega^n_{\mathrm{avg}\_k}, 0, 0, 0, 0, \ldots,0]^{\mathrm{T}}$, and $\boldsymbol{u}(t)\in\mathbb{R}^{m\times 1}$ stand for the input vector, respectively.

T-S fuzzy modeling approach represents the original nonlinear system in (4) by convex combination of a set of linear subsystem models, which is stated as follows.

Rule R^k: If z_1 is F^k_1, …, and z_u is F^k_u, the subsystem can be described as

$$\dot{\boldsymbol{x}}(t)=A_k\cdot\boldsymbol{x}(t)+B_k\cdot\boldsymbol{u}(t) \tag{5}$$

where $z_1,\ldots, z_u$ are functions of state variables; F^k_u denotes a fuzzy set of z_u or so-called membership function and r is the number of fuzzy rules, respectively; $A_k\in\mathbb{R}^{7n\times 7n}$, $B_k\in\mathbb{R}^{7n\times 7m}$ stand for system matrix the kth fuzzy subsystem, respectively.

By single point fuzzification, multiplicative reasoning and weighted average defuzzification, the T-S fuzzy model is expressed as

$$\dot{\boldsymbol{x}}(t)=\sum_{k=1}^{r}h_k\left(z_u\right)\cdot\left[A_k\cdot\boldsymbol{x}(t)+B_k\cdot\boldsymbol{u}(t)\right] \tag{6}$$

where $h_k\left(z_u\right)=\dfrac{\omega_k\left(z_u\right)}{\sum_{k=1}^{r}\omega_k\left(z_u\right)}$, and $\omega_k\left(z_u\right)=\prod_{q=1}^{u}F^k_u\left(z_u\right)$.

Thus, the kth membership function $h_k(z_u)$ satisfies

$$0\leqslant h_k\left(z_u\right)\leqslant 1,\quad \sum_{k=1}^{r}h_k\left(z_u\right)=1 \tag{7}$$

As a result, the T-S fuzzy model of the DCMGC with inclusion of the communication delay and the cyber-attacks (FDIAs) can be given by

$$\dot{\boldsymbol{x}}(t)=\sum_{k=1}^{r}h_k\left(z_u\right)\cdot\left[(F_k+A_k)\cdot\boldsymbol{x}(t)+A_{\mathrm{kd}}\cdot\boldsymbol{x}(t-\tau)+B_k\cdot\boldsymbol{u}(t)\right] \tag{8}$$

where τ including τ_{a} and τ_{T} that stands for acquisition delay and tertiary communication delay, respectively, and F_k and A_{kd} denote the FDIA matrix and the delay matrix, respectively.

B. Large Signal Stability Criteria

The Lyapunov direct method will be introduced to study the large signal stability of the T-S fuzzy mode [42], by which the Lyapunov function is defined as

$$V(\boldsymbol{x},t)=\boldsymbol{x}(t)^{\mathrm{T}}P\boldsymbol{x}(t) \tag{9}$$

where $P \in \mathbb{R}^{n\times n}$, and is a symmetric positive definite matrix.

The large signal stability of the system is sufficiently guaranteed if there exist a P satisfying

$$A_k^{\mathrm{T}} P + P A_k < 0 \tag{10}$$

Now, the stability criteria with time-delay and the cyber-attacks will be derived respectively from the mentioned Lyapunov direct method for the T-S fuzzy model of the DCMGC.

C. Stability Criterion With Time-Delay and Cyber-Attacks (FDIAs)

General stability criterion for the time-delay and the FDIAs, the T-S model in (8) will be reduced to

$$\dot{\boldsymbol{x}}(t) = \sum_{k=1}^{r} h_k(z_u) \cdot \left[(A_k + F_k)\boldsymbol{x}(t) + A_{k\mathrm{d}} \cdot \boldsymbol{x}(t-\tau) + B_k \cdot \boldsymbol{u}(t) \right] \tag{11}$$

Given the model in (13), large signal Lyapunov stability of the DCMGC will be determined by a series of LMIs that are expressed as

$$\begin{cases} P^{\mathrm{T}} = P > 0, Q_1^{\mathrm{T}} = Q_1 > 0, Q_2^{\mathrm{T}} = Q_2 > 0, \\ \begin{bmatrix} (1,1) & \tau P A_{\mathrm{d},i} & \tau P A_{\mathrm{d},i} \\ * & -Q_1 & 0 \\ * & 0 & -Q_2 \end{bmatrix} < 0 \end{cases} \tag{12}$$

where $(1,1) = P[(F + A_i) + A_{\mathrm{d},i}] + [(F + A_i) + A_{\mathrm{d},i}]^{\mathrm{T}} P + \tau(Q_1 + Q_2)$, and "*" represents transpose of the upper diagonal terms, respectively. Detailed derivation of (12) is given in the Appendix.

In the calculation of ROA, based on the T-S fuzzy modeling is used to linearize the nonlinear elements (e.g., CPL) in the DCMGC system to form a linear fuzzy set and the maximum and minimum deviation of the local linear subsystem is solved by the fuzzy rules from each linear subsystem, from which the LMIs can be obtained and solved. The existence of the positive definite matrix P guarantees asymptotical stability of the DCMGC in large signal notion with the time-delay and the cyber-attacks, and the stability region, i.e., the corresponding voltage and current values are substituted into the constructed Lyapunov function and ROA as well.

$$\begin{cases} V_i(x) = P_{i(i,i)} x_i^2 + \left[P_{i(i,2n+i)} + P_{i(2n+i,i)} \right] x_i x_{2n+i} + P_{i(2n+i,2n+i)} x_{2n+i}^2 \\ \mathrm{ROA}_i = \left\{ x : V_i(x) \leqslant V_{i\min}(x) \right\} \\ V_{i\min}(x) = V_{i\min}\left(\underbrace{0,\ldots,0}_{i-1}, x_i, \underbrace{0,\ldots,0}_{n-i}, \underbrace{0,\ldots,0}_{n}, \underbrace{0,\ldots,0}_{i-1}, \underbrace{0,\ldots,0}_{n-i}, x_{(2n+i)\min}, \underbrace{0,\ldots,0}_{n-i}, \underbrace{0,\ldots,0}_{4n} \right) \end{cases} \tag{13}$$

where, $x_i = -P_{i(i,2n+i)} \times x_{(2n+i)\min} / P_{i(i,i)}$, $i \leqslant n$.

IV. Large Signal Stability Analysis With Numerical Results

To check impact of the different component and parameters of on large signal stability, this section performs numerical results analysis of the ROA of the specific DCMGC that consists of three MGs as the topology in Figs. 1 and 2, and the main parameters are listed in Table I.

TABLE I
Parameters of the DCMGC Model

Components	Parameters	Value
Single DCMG	v^{β}_{bus} (β = 1,2,3)	48 V
	C^{b}_{ok} (β = 1,2,3; k = 1,2)	1000 μF
	r^{b}_{k} (β = 1,2,3; k = 1,2)	0.05 Ω
	L^{b}_{k} (β = 1,2,3; k = 1,2)	200 μH
	C^{b}_{bus} (β = 1,2,3)	2000 μF
	P^{b}_{CPL} (β = 1,2,3)	1 kW
Tie-lines	r^{b}_{T} (β = 1,2,3)	1 Ω
	L^{b}_{T} (β = 1,2,3)	500 μH
Hierarchical control	$K^{b}_{\mathrm{pIII},}$ (b = 1,2,3)	0.5
	$K^{b}_{\mathrm{pIII},}$ (β = 1,2,3)	10
	$K^{b}_{\mathrm{pII}\ k,}$ (β = 1,2,3, k = 1,2)	0.2
	$K^{b}_{\mathrm{iII}\ k,}$ (β = 1,2,3, k = 1,2)	10
	$K^{b}_{\mathrm{pv}\ k,}$ (β = 1,2,3, k = 1,2)	0.5
	$K^{b}_{\mathrm{iv}\ k,}$ (β = 1,2,3, k = 1,2)	20

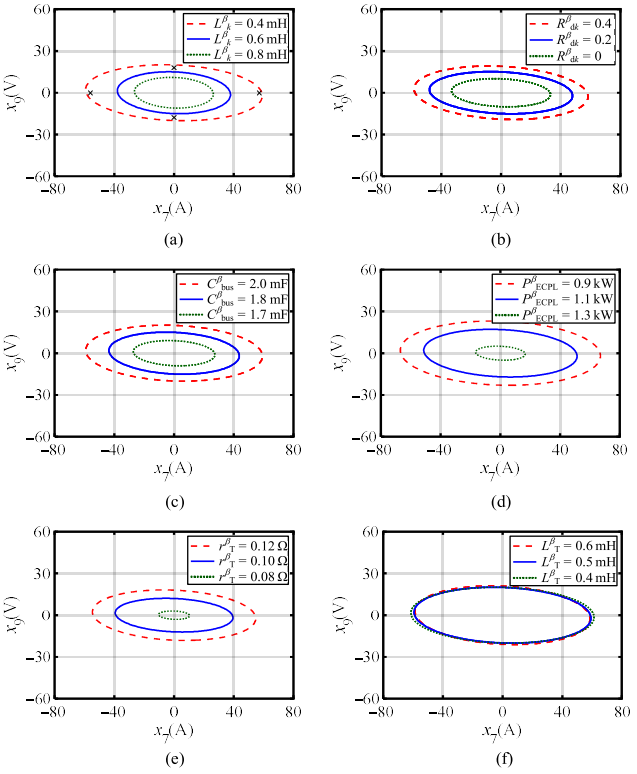

Fig. 3. Evolution of the ROA with changes of the circuit parameters. (a) Line inductance within DCMG. (b) Droop coefficient. (c) Bus capacitance. (d) CPL. (e) Resistance of the tie-lines. (f) Inductance of the tie-lines.

The evolution of the ROAs with varying parameters of the main circuit, hierarchical controller, communication delay and the FDIA for the DCMGC will be shown.

A. Influence of the Main Circuit Parameters

Fig. 3 shows the evolution of ROA of DCMGC β with variation of six parameters in the main circuit, viz., line inductance within DCMG, droop coefficient, bus capacitance,

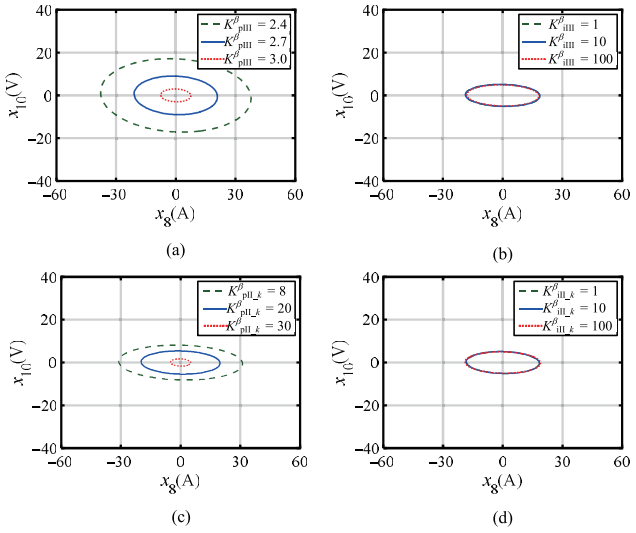

Fig. 4. Evolution of the ROA with different hierarchical control loop parameters. (a) Proportional gain of the tertiary controller. (b) Integral gain of the tertiary controller. (c) Proportional gain of the secondary controller. (d) Integral gain of the secondary controller.

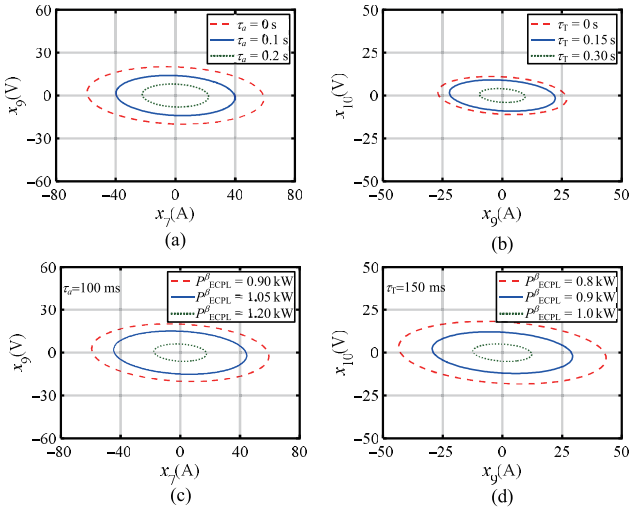

Fig. 5. Evolution of the ROA with time-delays. (a) Voltage acquisition delay. (b) Tertiary communication delay. (c) CPL with the voltage acquisition delay of τ_a = 100 ms. (d) CPL with the tertiary communication delay of τ_T = 150 ms.

CPL, the resistance of the tie-lines, and the inductance of the tie-lines, respectively. Specifically, the increase of the bus capacitance, droop coefficient and the resistance of the tie-line in the each DCMG will obviously enlarge the ROA, but the increase of the CPL and the equivalent line inductance will have a negative impact on the ROA. Moreover, the inductance of the tie-line has little effect on the ROA.

B. Influence of the Hierarchical Control

Fig. 4 depicts the ROA evolution of the system with different hierarchical control loop parameters. On both the tertiary and the secondary levels, the influence of the proportional gains ($K^{\beta}_{\mathrm{pIII}}$ and $K^{\beta}_{\mathrm{pII\_k}}$) in the two PI controllers is comparatively more significant than that of the integral gains. The smaller $K^{\beta}_{\mathrm{pIII}}$ or $K^{\beta}_{\mathrm{pII\_k}}$ the larger the ROA of the system, which means the better of the system stability. On the other hand, the changes of integral gains, i.e., $K^{\beta}_{\mathrm{iII\_k}}$ and $K^{\beta}_{\mathrm{iIII}}$ have little effect on the ROA of the DCMGC. The minor conclusion here is that the large signal stability of the DCMGC is primarily dependent on the proportional gains of the hierarchical controllers, in terms of the ROA.

C. Influence of the Time-Delays

Here, the time-delays over both the voltage acquisition in local MGs and the tertiary communications in the DCMGC are considered. As shown in Fig. 5(a) and (b), it is obvious that the time-delay in the voltage acquisition in local MGs has more significant impact than the tertiary communication delay on the ROA, and in both cases, larger time-delays will produce smaller ROAs.

To further check the influence of the time-delays on the large signal stability of the DCMGC, Fig. 5(c) and (d) shows the evolution of the ROA with CPL given the specific time-delay of

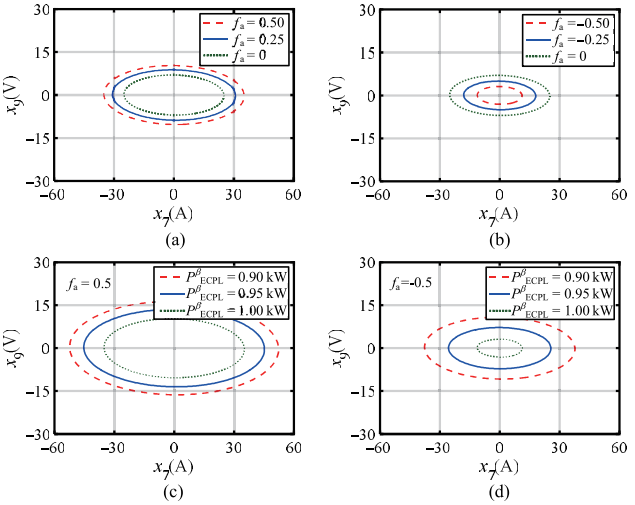

Fig. 6. Evolution of ROA with the FDIAs. (a) Positive coefficient. (b) Negative coefficient. (c) CPL under positive coefficient f_a = 0.5. (d) CPL under negative coefficient f_a = −0.5.

100 ms over the voltage acquisition in local MG and of 150 ms over the tertiary communications, respectively. Recall the ROA with varying CPL in Fig. 3(d) where the time-delays are not considered, the results here illustrate that the ROA shrinks with the time-delays.

D. Influence of the FDIAs

The evolution of the ROA of the DCMGC with the FDIAs is shown in Fig. 6, where the FDIAs with positive and with negative coefficient are given in Fig. 6(a) and (b), respectively. For comparison, the DCMGC is not attacked with f_a = 0, and the ROA of the system becomes small with negative f_a, indicating that the system stability becomes worse, while the ROA of the system becomes larger with positive f_a, indicating

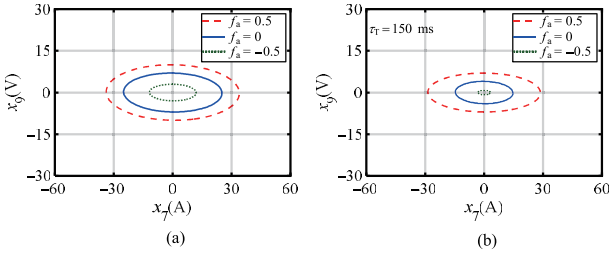

Fig. 7. Evolution of ROA with the FDIAs and time-delay simultaneously. (a) The FDIAs with different coefficient but without time-delays and (b) with both FDIAs and the time-delay.

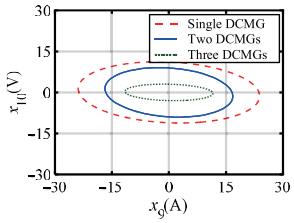

Fig. 8. Evolution of the ROA with changes of the structure of the system.

the improvement of the system stability.

The varying trend of the ROA with changing CPL for the FDIAs with positive and negative coefficient are also shown in Fig. 6(c) and (d), respectively, which also demonstrates the difference between opposite signs of the attack coefficient.

E. Combined Influence of the FDIAs and Time-Delays

Fig. 7 shows the evolution of ROA of the FDIAs and time-delay simultaneously. For comparison, the DCMGC under different attack coefficient but without time-delays is given in Fig. 7(a), while with both FDIAs and tertiary communication time-delays in Fig. 7(b), respectively. Specifically, the tertiary communication time-delay is given as $\tau_r = 150$ ms. It is obvious that the tertiary communication delay has a worsening impact on the ROA of DCMGC subject to the FDIAs.

F. Influence of the Change of System Structure

For the transient that the transition from islanded to interconnected mode, the corresponding order of the overall equivalent model will be changed, and the matrices or the sub-matrices involved for the large signal stability will be updated as well. The influence of the transition of islanded mode to interconnected mode on the ROA of the system is illustrated in Fig. 8 where the ROA is reduced with that transition and is reduced further with three DCMGs are interconnected, which means that the more DCMGs are interconnected, the more reduced damping of the system, and therefore the weaker the system stability.

G. Comparison Between Actual ROA and Estimated ROA

Conservatism is an inherent problem with existing methods for large signal stability analysis of DCMG systems, and it may vary from case to case. The comparison between the actual ROA and the estimated ROA for the DCMGC is shown in Fig. 6 where the estimated ROA is slightly smaller than the actual ROA, which means that the estimated result is arguably acceptable in this case.

H. Comparison Between the T-S Fuzzy Modeling and the Sums-of-Squares (SOS)

The comparison between the T-S fuzzy modeling and the sums-of-squares (SOS) for the large signal stability of the DCMGC is shown in Fig. 4, where the T-S method outperforms the SOS in terms of the estimated stability region (ROA). Therefore, the conservatism of T-S method is lower than that of the SOS in this case.

In addition, we have also noticed that some existing works, e.g., the results in [43] claim that the SOS is better than T-S for the PLL stability in VSCs, which may be true for the lower order models of the VSCs, but not be case for higher order complex systems like DCMGCs, and even the solvability of the SOS in higher order system models remains unclear. The benchmark testing systems for comparisons among the existing large signal stability methods opens research topics in future studies.

V. Experimental Results

To verify the large signal stability analysis with numerical results for the DCMGC, the hardware-in-the-loop experimental results are provided. In the set-up, every MG in the experiments is composed of two parallel DC-DC buck converters, and therefore there are six buck converters of three MGs in the DCMGC. The equivalent parameters are consistent with the numerical analysis above. The experimental verification will be going through multiple testing scenarios, including response to tertiary control, transition of DCMGs from stand-alone to interconnected operation, time-delays, and FDIAs.

To verify the conservatism of the estimated ROA, three testing points are picked, viz., point A, B, and C in Fig. 9, from which point A and B are well within both ROAs, whereas point C is on the verge of the actual ROA but out of the estimated ROA. Through the stability criterion, the sufficient condition for the large signal stability of the system is $P < 1.1566$ kW.

Fig. 10 shows the comparison between the T-S fuzzy modeling and the SOS in terms of ROA.

Fig. 11 shows the transient response to the tertiary control from disabled to enabled state for the DCMGC. The DCMGC was initially operating without tertiary control, and the output power of the three MGs are 1.2, 1.3, and 1.4 kW, respectively. The tertiary control is then enabled after 25 s, and the global power sharing among the three MG is achieved through the power flow over the tie-lines.

Fig. 12 shows experimental results of the MGs from the stand-alone to the interconnected DCMGC. The two DCMGs were initially operating independently, and they behave stably

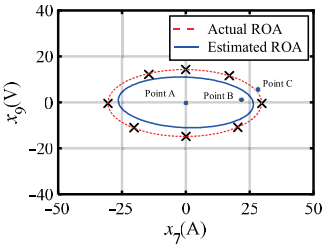

Fig. 9. Comparison of the actual ROA and estimated ROA.

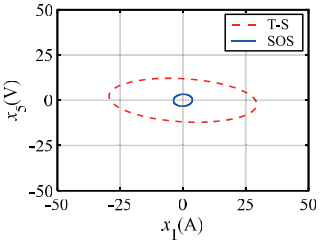

Fig. 10. Comparison between the T-S fuzzy modeling and the SOS in terms of ROA.

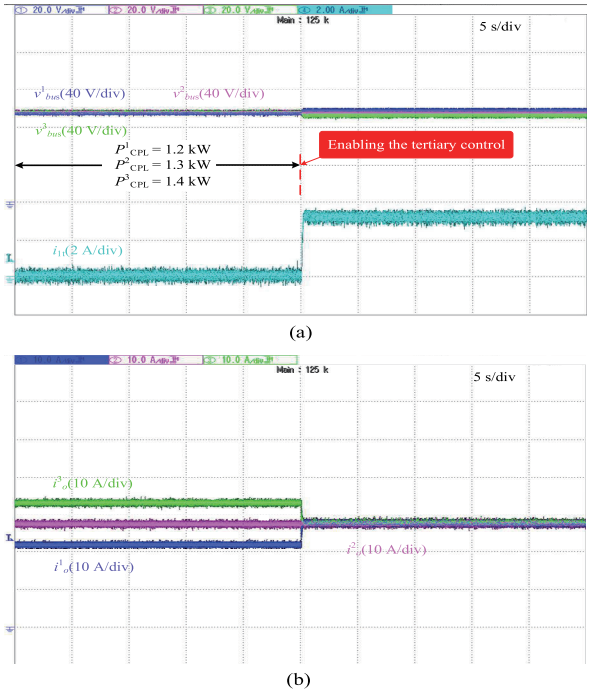

Fig. 11. Experimental results of the response to the tertiary control of the DCMGC. (a) Bus voltage and the tie-line current. (b) Output current of every DCMG in the network.

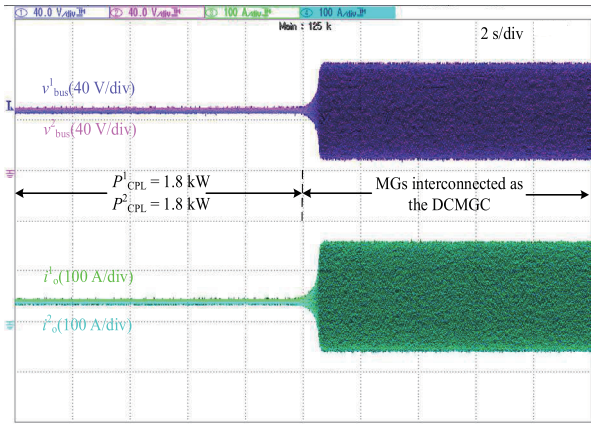

Fig. 12. Experimental results of the transition of MGs from stand-alone to the interconnected DCMGC.

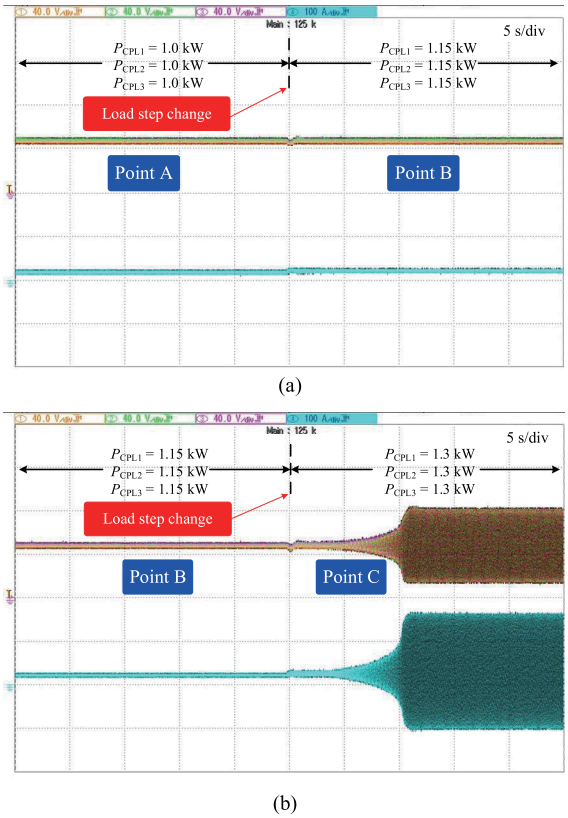

Fig. 13. Experimental results of the conservatism analysis based on T-S fuzzy modeling. (a) P^{β}_{CPL} = 1.0 kW to P^{β}_{CPL} = 1.15 kW. (b) P^{β}_{CPL} = 1.15 kW to P^{β}_{CPL} = 1.3 kW.

in this mode. However, the system experiences the oscillation that means unstable operation in the interconnection after 10 s of the stand-alone operation. This result agrees well with the previous analysis that interconnection reduces the damping of the DCMGs and contributes to the instability of the system.

Fig. 13 shows experimental results with the load step changes, where in Fig. 13(a), the DCMGC retains large signal stability subject to the load step transient from point A to B, i.e., $P^1_{CPL} = P^2_{CPL} = P^3_{CPL}$ = 1.0 kW to $P^1_{CPL} = P^2_{CPL} = P^3_{CPL}$ = 1.15 kW, and the load transient from point B to C in Fig. 13(b), $P^1_{CPL} = P^2_{CPL} = P^3_{CPL}$ = 1.15 kW to $P^1_{CPL} = P^2_{CPL} = P^3_{CPL}$ = 1.3 kW, respectively. Obviously, the DCMGC undergoes stable response in Fig. 13(a) and witnesses high oscillation in Fig. 13(b), respectively, which corroborates the acceptable conservatism of the estimated ROA by the T-S modeling method.

Fig. 14 shows experimental results with the tertiary control. In Fig. 14 (a), the DCMGC retains large signal stability subject

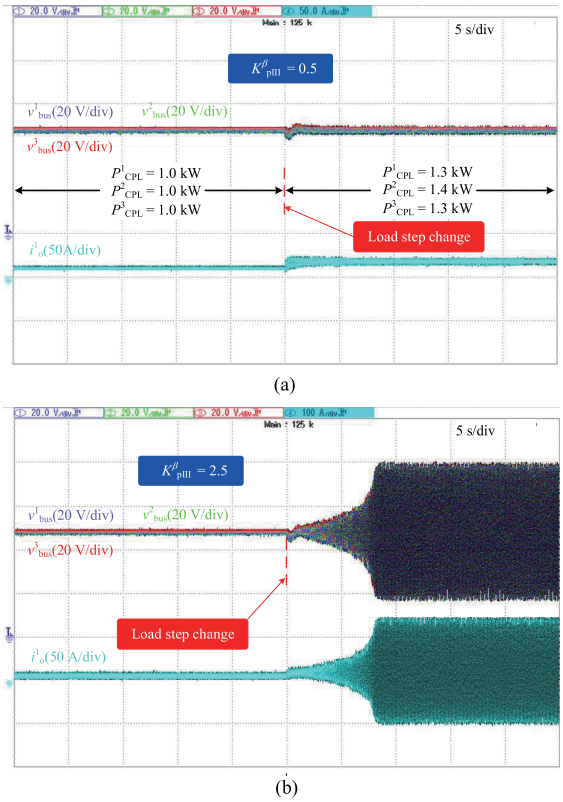

Fig. 14. Experimental results of the response to proportional gain of the tertiary control of the DCMGC: (a) $K^{\beta}_{pIII} = 0.5$ and (b) $K^{\beta}_{pIII} = 2.5$.

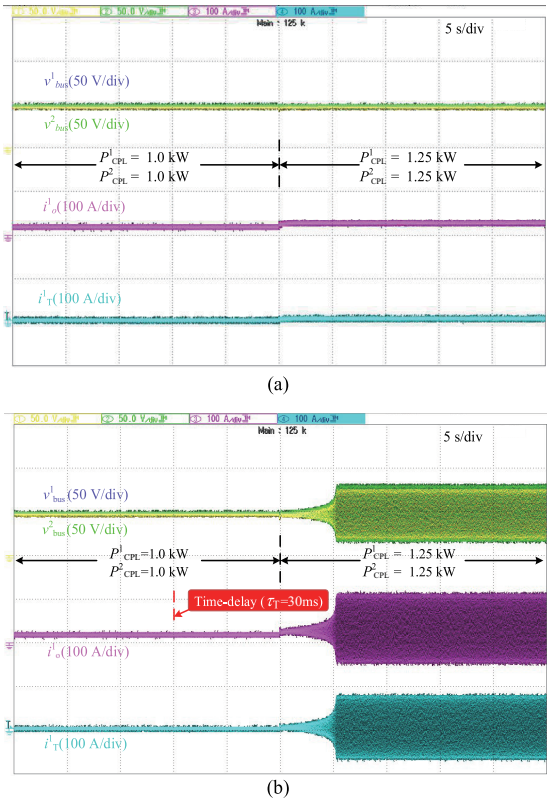

Fig. 16. Experimental results with the communication time-delay. (a) Bus voltage, output current and tie-line current without time-delay and (b) with time-delay.

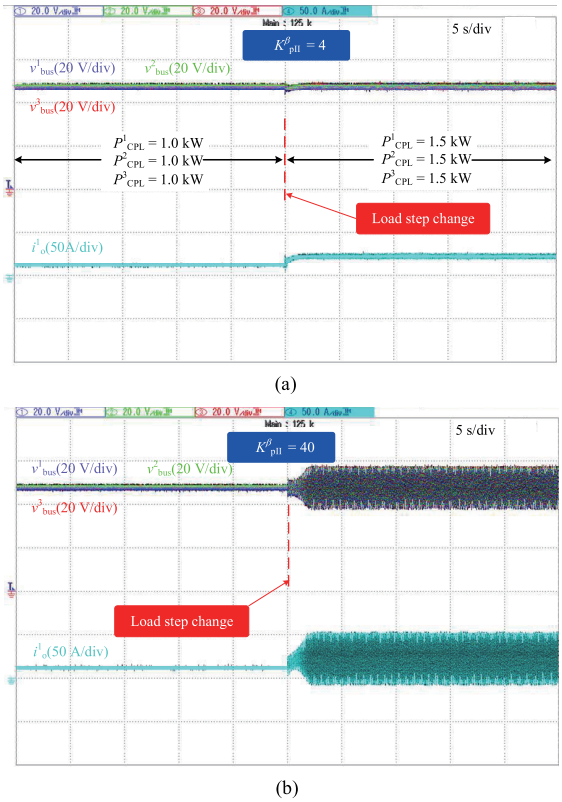

Fig. 15. Experimental results of the response to proportional gain of the secondary control of the DCMGC: (a) $K^{\beta}_{pII} = 4$ and (b) $K^{\beta}_{pII} = 40$.

to the load step transient, i.e., $P^1_{CPL} = P^2_{CPL} = P^3_{CPL} = 1.0$ kW to $P^1_{CPL} = P^3_{CPL} = 1.3$ kW and $P^2_{CPL} = 1.4$ kW, respectively. By comparison in Fig. 14 (b), the DCMGC witness oscillation although subject to the same load transient as in Fig 14 (a), but the tertiary control gain has been increased from 0.5 to 2.5. Thus, the large signal stability is deteriorated by the higher proportional gain of the tertiary controller.

Fig. 15 shows the experimental results with the secondary control. In Fig. 15 (a), the DCMGC retains large signal stability subject to the load step transient, i.e., $P^1_{CPL} = P^2_{CPL} = P^3_{CPL} = 1.0$ kW to $P^1_{CPL} = P^2_{CPL} = P^3_{CPL} = 1.5$ kW, respectively. However, in Fig. 15 (b) with increased secondary control gain from 4 to 40, the DCMGC witness oscillation although subject to the same load transient as in Fig. 15(a). Thus, the large signal stability is deteriorated by the higher proportional gain of the secondary controller.

Fig. 16 shows experimental results with the communication time-delay. For comparison, the response to the same load transient without the time-delay is given in Fig. 16(a), and that with the time-delay in Fig. 16(b), respectively. One can observe that the DCMGC is operating stably to the transient of increasing the CPL from 1.0 kW to 1.25 kW without the time-delay, but finally experiences oscillation after adding the time-delay of 30 ms, although with the same CPL transient.

The validation of the influence of the FDIAs on the large signal stability of the DCMGC will be shown in terms of the

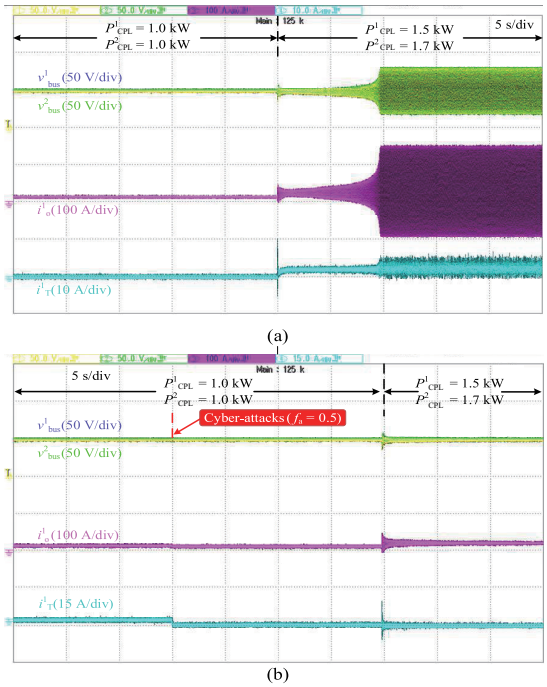

Fig. 17. Experimental results with the FDIA of positive coefficient. (a) Bus voltage, output current and tie-line current without the attack and (b) with the attack.

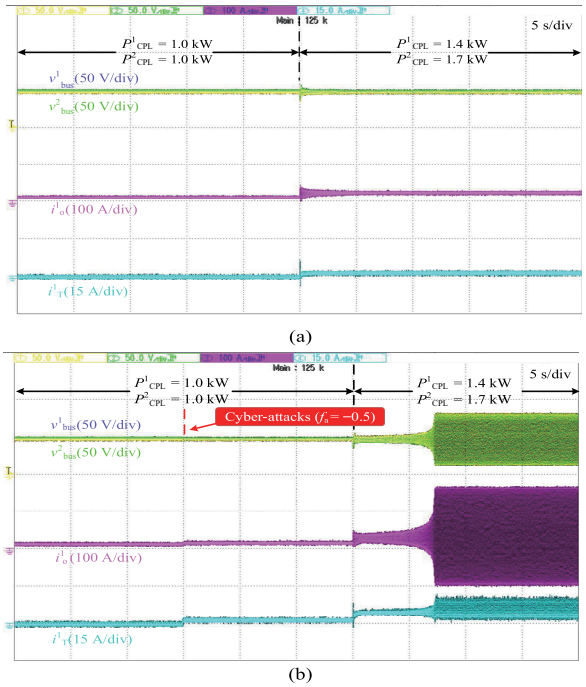

Fig. 18. Experimental results with the FDIA of negative coefficient. (a) Bus voltage, output current and tie-line current without the attack and (b) With the attack.

positive and negative attack coefficient in Figs. 17 and 18, respectively.

Fig. 17 describes experimental results with the FDIA of the positive coefficient, i.e., f_a = 0.5. In Fig. 17(a), the DCMGC is pushed into oscillation subject to the load step transient, i.e., $P^1_{CPL} = P^2_{CPL}$ =1.0 kW to P^1_{CPL} = 1.5 kW and P^2_{CPL} = 1.7 kW, respectively. By comparison in Fig. 17(b), the DCMGC remains stable with the FDIA although subject to the same load transient as just before. The improvement of the large signal stability by the FDIA with the positive coefficient agrees well with the numerical results in Section IV.

Again, Fig. 18 shows experimental results with the FDIA of the negative coefficient, i.e., f_a = −0.5. In Fig. 18(a), the DCMGC retains large signal stability subject to the load step transient, i.e., $P^1_{CPL} = P^2_{CPL}$ = 1.0 kW to P^1_{CPL} = 1.4 kW and P^2_{CPL} = 1.7 kW, respectively. By comparison in Fig. 18 (b), the DCMGC witness oscillation although subject to the same load transient as in Fig 18(a). Therefore, the deterioration of the large signal stability by the FDIA with the negative coefficient is in line with the numerical results in Section IV as well.

VI. Conclusions

This work investigates the large signal stability of DCMGCs for the first time from the perspective of CPS. Based on the T-S fuzzy modeling approach, the ROA of the system under various conditions, e.g., the main circuit parameters, the hierarchical control, the time-delays, and the cyber-attacks, has been estimated, which is corroborated by the experimental results. Conclusions of the work can be drawn as follows:

(1) It has been found that not only the main circuit parameters have significant impact on the large signal stability, but also the hierarchical control and the communications play significant roles in affecting the stability of the DCMGC.

(2) In the hierarchical control, the proportional gains of the tertiary and the secondary control has a more significant impact than the integral gains on the large signal stability, and the droop coefficient in the primary control also has a significant impact on the large signal stability of the system.

(3) The time-delays in the voltage acquisition and over the tertiary communications reduce the large signal stability, and the ROA with the time-delay in the former case is larger than that in the latter.

(4) The cyber-attacks (FDIAs) impact differently in terms of the attack coefficient on the large signal stability, and specifically the FDIAs with positive coefficient increase the ROA whereas the FDIAs with negative coefficient decrease the ROA.

Appendix
Derivation of the Stability Criterion in (12)

With the time-delayed and the FDIAs T-S fuzzy model in (11), its subsystem model is given by

$$\dot{\boldsymbol{x}}(t) = (F + A)\boldsymbol{x}(t) + A_d\,\boldsymbol{x}(t-\tau) \tag{14}$$

where $x(t–\tau)$ satisfying the Newton-Leibniz equation that is expressed as

$$\int_{t-\tau}^{t} \dot{\boldsymbol{x}}(s)\mathrm{d}s = \boldsymbol{x}(t) - \boldsymbol{x}(t-\tau) \tag{15}$$

Thus, (14) can be transformed as

$$\dot{\boldsymbol{x}}(t) = [(F + A) + A_{\mathrm{d}}]\boldsymbol{x}(t) - A_{\mathrm{d}}\int_{t-\tau}^{t}[(F+A)\boldsymbol{x}(s)+A_{\mathrm{d}}\boldsymbol{x}(s-\tau)]\mathrm{d}s \quad (16)$$

By Lyapunov stability theory, the Lyapunov-Krasovskii functional in this case can be written as

$$\begin{aligned} V(t) = \boldsymbol{x}(t)^{\mathrm{T}} P\,\boldsymbol{x}(t) + \int_{-\tau}^{0}\int_{t+\theta}^{t}\boldsymbol{x}(s)^{\mathrm{T}} Q_1\boldsymbol{x}(s)\mathrm{d}s\mathrm{d}\theta + \\ \int_{-2\tau}^{-\tau}\int_{t+\theta}^{t}\boldsymbol{x}(s)^{\mathrm{T}} Q_2\boldsymbol{x}(s)\mathrm{d}s\mathrm{d}\theta, P = P^{\mathrm{T}} > 0 \end{aligned} \quad (17)$$

where $Q_1 = Q_1^{\mathrm{T}} > 0$ and $Q_2 = Q_2^{\mathrm{T}} > 0$, respectively.

Finding the derivative of (17) yields

$$\begin{aligned} \dot{V}(t) = \boldsymbol{x}(t)^{\mathrm{T}}\{[(F + A) + A_{\mathrm{d}}]^{\mathrm{T}} P + P[(F + A) + A_{\mathrm{d}}] + \tau(Q_1 + Q_2)\}\boldsymbol{x}(t) - \\ 2\int_{t-\tau}^{t}\boldsymbol{x}(t)^{\mathrm{T}} PA_{\mathrm{d}} A\boldsymbol{x}(s)\mathrm{d}s - 2\int_{t-\tau}^{t}\boldsymbol{x}(t)^{\mathrm{T}} PA_{\mathrm{d}} A_{\mathrm{d}}\boldsymbol{x}(s-\tau)\mathrm{d}s - \\ \int_{t-\tau}^{t}\boldsymbol{x}(s)^{\mathrm{T}} Q_1\boldsymbol{x}(s)ds - \int_{t-\tau}^{t}\boldsymbol{x}(s-\tau)^{\mathrm{T}} Q_2\boldsymbol{x}(s-\tau)\mathrm{d}s \end{aligned} \quad (18)$$

To simplify (18), the bounding inequality is given by

$$\gamma_1^{\mathrm{T}}\gamma_2 + \gamma_2^{\mathrm{T}}\gamma_1 \leqslant \gamma_1^{\mathrm{T}} W^{-1}\gamma_1 + \gamma_2^{\mathrm{T}} W\gamma_2, W = W^{\mathrm{T}} > 0 \quad (19)$$

where γ_1 and γ_2 can be matrices or vectors, and W is a symmetric positive definite matrix of appropriate dimensions, respectively.

Now, (18) can be rewritten as

$$\begin{aligned} \dot{V}(t) = \boldsymbol{x}(t)^{\mathrm{T}}\{[(F + A) + A_{\mathrm{d}}]^{\mathrm{T}} P + P[(F + A) + A_{\mathrm{d}}] + \tau(Q_1 + Q_2)\}\boldsymbol{x}(t) + \\ \int_{t-\tau}^{t}\boldsymbol{x}(t)^{\mathrm{T}} PA_{\mathrm{d}} X_1^{-1} A_{\mathrm{d}}^{\mathrm{T}} P\boldsymbol{x}(t)\mathrm{d}s + \int_{t-\tau}^{t}\boldsymbol{x}(s)^{\mathrm{T}} A^{\mathrm{T}} X_1 A\boldsymbol{x}(s)\mathrm{d}s - \\ \int_{t-\tau}^{t}\boldsymbol{x}(s)^{\mathrm{T}} Q_1\boldsymbol{x}(s)\mathrm{d}s - \int_{t-\tau}^{t}\boldsymbol{x}(s-\tau)^{\mathrm{T}} A_{\mathrm{d}}^{\mathrm{T}} X_2 A_{\mathrm{d}}\boldsymbol{x}(s-\tau)\mathrm{d}s + \\ \int_{t-\tau}^{t}\boldsymbol{x}(t)^{\mathrm{T}} PA_{\mathrm{d}} X_2^{-1} A_{\mathrm{d}}^{\mathrm{T}} P\boldsymbol{x}(t)\mathrm{d}s + \int_{t-\tau}^{t}\boldsymbol{x}(s-\tau)^{\mathrm{T}} Q_2\boldsymbol{x}(s-\tau)\mathrm{d}s \end{aligned} \quad (20)$$

Let $Q_1 = A^{\mathrm{T}} X_1 A$ and $Q_2 = A_{\mathrm{d}}^{\mathrm{T}} X_2 A_{\mathrm{d}}$, and combing with (19), thus (20) can be reduced to

$$\begin{aligned} \dot{V}(t) \leqslant \boldsymbol{x}(t)^{\mathrm{T}}\{[(F + A) + A_{\mathrm{d}}]^{\mathrm{T}} P + P[(F + A) + A_{\mathrm{d}}] + \tau(Q_1 + Q_2)\}\boldsymbol{x}(t) + \\ \tau(PA_{\mathrm{d}} X_1^{-1} A_{\mathrm{d}}^{\mathrm{T}} P) + \tau(PA_{\mathrm{d}} X_2^{-1} A_{\mathrm{d}}^{\mathrm{T}} P) \end{aligned} \quad (21)$$

Using Schur-complement, one can write (21) as

$$\dot{V}(t) \leqslant \boldsymbol{x}(t)^{\mathrm{T}}\begin{bmatrix} (1,1) & \tau PA_{\mathrm{d}} & \tau PA_{\mathrm{d}} \\ * & -X_1 & 0 \\ * & 0 & -X_2 \end{bmatrix}\boldsymbol{x}(t) \quad (22)$$

where $(1,1) = P[(F + A_i) + A_{\mathrm{d},i}] + [(F + A_i) + A_{\mathrm{d},i}]^{\mathrm{T}} P + \tau(Q_1 + Q_2)$.

To guarantee the asymptotic stability of the system (14) or equivalently (16), it is required that $\dot{V}(t) < 0$, which means the following LMI is satisfied as

$$\begin{bmatrix} (1,1) & \tau PA_{\mathrm{d}} & \tau PA_{\mathrm{d}} \\ * & -Q_1 & 0 \\ * & 0 & -Q_2 \end{bmatrix} < 0 \quad (23)$$

With this, the derivation is completed.

Reference

[1] L. Meng, Q. Shafiee, G. F. Trecate, H. Karimi, D. Fulwani, X. Lu, and J. M. Guerrero, "Review on control of DC microgrids and multiple microgrid clusters," in *IEEE Journal of Emerging and Selected Topics in Power Electronics*, vol. 5, no. 3, pp. 928–948, 2017.

[2] H. Kakigano, Y. Miura, and T. Ise, "Low-voltage bipolar-type DC microgrid for super high quality distribution," in *IEEE Transactions on Power Electronics*, vol. 25, no. 12, pp. 3066–3075, Dec. 2010.

[3] Q. Shafiee, T. Dragičević, J. C. Vasquez, and J. M. Guerrero, "Hierarchical control for multiple DC-microgrids clusters," in *IEEE Transactions on Energy Conversion*, vol. 29, no. 4, pp. 922–933, Dec. 2014.

[4] R. Olfati-Saber, J. A. Fax, and R. M. Murray, "Consensus and cooperation in networked multi-agent systems," in *Proceedings of the IEEE*, vol. 95, no. 1, pp. 215–233, Jan. 2007.

[5] V. Nasirian, S. Moayedi, A. Davoudi, and F. L. Lewis, "Distributed cooperative control of DC microgrids," in *IEEE Transactions on Power Electronics*, vol. 30, no. 4, pp. 2288–2303, Apr. 2015.

[6] P. Wang, X. Lu, X. Yang, W. Wang, and D. Xu, "An improved distributed secondary control method for DC microgrids with enhanced dynamic current sharing performance," in *IEEE Transactions on Power Electronics*, vol. 31, no. 9, pp. 6658–6673, Sept. 2016.

[7] Y. Li, P. Dong, M. Liu, and G. Yang, "A distributed coordination control based on finite-time consensus algorithm for a cluster of DC microgrids," in *IEEE Transactions on Power Systems*, vol. 34, no. 3, pp. 2205–2215, May 2019.

[8] J. V. D. Keybus, G. Deconinck, and R. Belmans, "Agora: Distributed tertiary control of distributed resources," in *Proceedings of 15th Power Systems Computation Conference, PSCC 2005*, Liege, Belgium, 2005: Power Systems Computation Conference (PSCC).

[9] A. Bidram and A. Davoudi, "Hierarchical structure of microgrids control system," in *IEEE Transactions on Smart Grid*, vol. 3, no. 4, pp. 1963–1976, Dec. 2012.

[10] S. Moayedi and A. Davoudi, "Distributed tertiary control of DC microgrid clusters," in *IEEE Transactions on Power Electronics*, vol. 31, no. 2, pp. 1717–1733, Feb. 2016.

[11] A. Manur, M. Marathe, and G. Venkataramanan, "A distributed approach for secondary and tertiary layer control in DC microgrids," in *Proceedings of 2020 IEEE Energy Conversion Congress and Exposition (ECCE)*, Detroit, MI, USA, 2020, pp. 1284–1291.

[12] T. Takagi and M. Sugeno, "Fuzzy identification of systems and its applications to modeling and control," in *IEEE Transactions on Systems, Man, and Cybernetics*, vol. SMC-15, no. 1, pp. 116–132, Jan.-Feb., 1985.

[13] R. K. Brayton and J. K. Moser, "A theory of nonlinear networks. I," in *Quarterly of Applied Mathematics*, vol. 22, no. 1, pp. 1–33, 1964.

[14] R. Genesio, M. Tartaglia, and A. Vicino, "On the estimation of asymptotic stability regions: State of the art and new proposals," in *IEEE Transactions on Automatic Control*, vol. 30, no. 8, pp. 747–755, Aug. 1985.

[15] M. Belkhayat, R. Cooley, and A. Witulski, "Large signal stability criteria for distributed systems with constant power loads," in *Proceedings of PESC '95 - Power Electronics Specialist Conference*, Atlanta, GA, USA, 1995, pp. 1333–1338, vol. 2 .

[16] H. J. Kim, S. W. Kang, G. S. Seo, P. Jang, and B. H. Cho,"Large-signal stability analysis of DC power system with shunt active damper," in *IEEE Transactions on Industrial Electronics*, vol. 63, no. 10, pp. 6270–6280, Oct. 2016.

[17] X. Liu and Y. Bian, "Large signal stability analysis of the DC microgrid with the storage system," in *Proceedings of 2017 20th International Conference on Electrical Machines and Systems (ICEMS)*, 2017, pp. 1–5.

[18] F. Chang, X. Cui, M. Wang, W. Su, and A. Q. Huang, "Large-signal stability criteria in DC power grids with distributed-controlled converters and constant power loads," in *IEEE Transactions on Smart Grid*, vol. 11, no. 6, pp. 5273–5287, Nov. 2020.

[19] J. Jiang, F. Liu, S. Pan, X. Zha, W. Liu, C. Chen, and L. Hao, "A conservatism-free large signal stability analysis method for DC microgrid based on mixed potential theory," in *IEEE Transactions on Power Electronics*, vol. 34, no. 11, pp. 11342–11351, Nov. 2019.

[20] F. Chang, X. Cui, M. Wang, and W. Su, "Potential-based large-signal stability analysis in DC power grids with multiple constant power loads," in *IEEE Open Access Journal of Power and Energy*, vol. 9, pp. 16–28, 2022.

[21] Z. Liu, X. Ge, M. Su, H. Han, W. Xiong, and Y. Gui, "Complete large-signal stability analysis of DC distribution network via Brayton-Moser's mixed potential theory," in *IEEE Transactions on Smart Grid*, vol. 14, no. 2, pp. 866–877, 2023.

[22] W. Xie, M. Han, W. Cao, J. M. Guerrero, and J. C. Vasquez, "System-level large-signal stability analysis of droop-controlled DC microgrids," in *IEEE Transactions on Power Electronics*, vol. 36, no. 4, pp. 4224–4236, Apr. 2021.

[23] M. Su, Z. Liu, Y. Sun, H. Han, and X. Hou, "Stability analysis and stabilization methods of DC microgrid with multiple parallel-connected DC-DC converters loaded by CPLs," in *IEEE Transactions on Smart Grid*, vol. 9, no. 1, pp. 132–142, Jan. 2018.

[24] A. A. Eajal, A. H. Yazdavar, E. F. El-Saadany, and K. Ponnambalam, "On the load ability and voltage stability of islanded AC-DC hybrid microgrids during contingencies," in *IEEE Systems Journal*, vol. 13, no. 4, pp. 4248–4259, Dec. 2019.

[25] A. P. N. Tahim, D. J. Pagano, E. Lenz, and V. Stramosk, "Modeling and stability analysis of islanded DC microgrids under droop control," in *IEEE Transactions on Power Electronics*, vol. 30, no. 8, pp. 4597–4607, 2015.

[26] G. Qi, A. Chen, and J. Chen,"Improved control strategy of interlinking converters with synchronous generator characteristic in islanded hybrid AC/DC microgrid," in *CPSS Transactions on Power Electronics and Applications*, vol. 2, no. 2, pp. 149–158, 2017.

[27] M. Mao, C. Qian, and Y. Ding,"Decentralized coordination power control for islanding microgrid based on PV/BES-VSG," in *CPSS Transactions on Power Electronics and Applications*, vol. 3, no. 1, pp. 14–24, Mar. 2018.

[28] H.-J. Kim, S.-W. Kang, G.-S. Seo, P. Jang, and B.-H. Cho, "Large-signal stability analysis of DC power system with shunt active damper," in *IEEE Transactions on Industrial Electronics*, vol. 63, no. 10, pp. 6270–6280, Oct. 2016.

[29] J. Ming, Y. Wang, F. Wang, and B. Su, "Large-signal stability analysis and shunt active damper compensation for DC microgrid with multiple constant power loads," in *Proceedings of 2019 22nd International Conference on Electrical Machines and Systems (ICEMS)*, 2019, pp. 1–6.

[30] P. Lin, C. Zhang, P. Wang, and J. Xiao, "A decentralized composite controller for unified voltage control with global system large-signal stability in DC microgrids," in *IEEE Transactions on Smart Grid*, vol. 10, no. 5, pp. 5075–5091, Sept. 2019.

[31] R. Han, M. Tucci, A. Martinelli, J. M. Guerrero, and G. Ferrari-Trecate, "Stability analysis of primary plug-and-play and secondary leader-based controllers for DC microgrid clusters," in *IEEE Transactions on Power Systems*, vol. 34, no. 3, pp. 1780–1800, May 2019.

[32] S. Liu, X. Li, M. Xia, Q. Qin, and X. Liu, "Takagi-sugeno multimodeling-based large signal stability analysis of DC microgrid clusters," in *IEEE Transactions on Power Electronics*, vol. 36, no. 11, pp. 12670–12684, 2021.

[33] C. Dong, H. Jia, Q. Xu, J. Xiao, Y. Xu, P. Tu, P. Lin, X. Li, and P. Wang, "Time-delay stability analysis for hybrid energy storage system with hierarchical control in DC microgrids," in *IEEE Transactions on Smart Grid*, vol. 9, no. 6, pp. 6633–6645, 2018.

[34] G. Lou, W. Gu, Y. Xu, W. Jin, and X. Du, "Stability robustness for secondary voltage control in autonomous microgrids with consideration of communication delays," in *IEEE Transactions on Power Systems*, vol. 33, no. 4, pp. 4164–4178, Jul. 2018.

[35] X. Wu, Y. Xu, J. He, C. Shen, and J. M. Guerrero, "Delay-dependent small-signal stability analysis and compensation method for distributed secondary control of microgrids," in *IEEE Access*, vol. 7, pp. 170919–170935, 2019.

[36] W. Yao, Y. Wang, Y. Xu, and C. Dong, "Small-signal stability analysis and lead-lag compensation control for DC networked-microgrid under multiple time delays," in *IEEE Transactions on Power Systems*, vol. 38, no. 1, pp. 921–933, 2023.

[37] R. Fu, X. Huang, J. Sun, Z. Zhou, D. Chen, and Y. Wu, "Stability analysis of the cyber physical microgrid system under the intermittent DoS attacks," in *Energies*, vol. 10, no. 5, 2017.

[38] A. Y. Lu and G. H. Yang, "Stability analysis for cyber-physical systems under denial-of-service attacks," in *IEEE Transaction on Cybernetics*, vol. 51, no. 11, pp. 5304–5313, Nov. 2021.

[39] M. Leng, S. Sahoo, F. Blaabjerg, and M. Molinas, "Projections of cyber attacks on stability of DC microgrids—modeling principles and solution," in *IEEE Transactions on Power Electronics*, vol. 37, no. 10, pp. 11774–11786, 2022.

[40] M. S. Sadabadi, S. Sahoo, and F. Blaabjerg, "Stability oriented design of cyber attack resilient controllers for cooperative DC microgrids," in *IEEE Transactions on Power Electronics*, vol. 37, no. 2, pp. 1310–1321, Jan. 2022.

[41] S. Sanchez and M. Molinas, "Large signal stability analysis at the common coupling point of a DC microgrid: A grid impedance estimation approach based on a recursive method," in *IEEE Transactions on Energy Conversion*, vol. 30, no. 1, pp. 122–131, Mar. 2015.

[42] K. Tanaka and M. Sugeno, "Stability analysis and design of fuzzy control systems," in *Fuzzy Sets and Systems*, vol. 45, no. 2, pp. 135–156, 1992.

[43] X. Li, Z. Wang, Y. Liu, Z. Wang, L. Zhu, L. Guo, C. Zhang, and C. Wang, "The largest estimated domain of attraction and its applications for transient stability analysis of PLL synchronization in weak-grid-connected VSCs," in *IEEE Transactions on Power Systems*, vol. 38, no. 5, pp. 4107–4121, 2022.

Sucheng Liu received Ph. D. degree in electrical engineering from Chongqing University, Chongqing, China, in 2013. He is currently a Full Professor with the School of Electrical and Information Engineering, Anhui University of Technology. He was a Visiting Research Associate with Queen's University, Kingston, Ontario, Canada, where he conducted two research projects sponsored by GE and NSERC, from Feb. 2015 to Feb. 2016. His research interests include modeling and control of DC microgrids and clusters and switching power converters. He has published more than 60 refereed journal and conference papers and holds 16 patents and has 4 patents pending.

Dr. Liu is an IEEE Member, a CPSS Member, and a Member of IEEE Power Electronics Society. He also serves as an active reviewer for a dozen of international Journals and Conferences, such as *IEEE Transactions on Power Electronics, IEEE Journal of Emerging and Selected Topics in Power Electronics, IEEE Open Journal of Power Electronics, IEEE Transactions on Industrial Electronics*, etc. He served as TPC members and Session Chairs for multiple conferences. He received Best Paper Awards at the IEEE International Conference on Predictive Control of Electrical Drives and Power Electronics (PRECEDE), Jinan, China, in 2021, IEEE International Conference on DC Microgrids (ICDCM), Matsue, Japan, in 2019, and the China Power Supply Society Conference (CPSSC), Shanghai, China, in 2017, respectively.

Chao Fang was born in Anhui, China, in 1996. He received the B.S. degree in electrical engineering and automation from Chuzhou University in 2020. He is currently working toward the M.S. degree in electrical engineering at Anhui University of Technology. His research interests include large signal stability analysis of DC microgrid clusters under cyber-physical systems perspective, and distributed control.

Xuefeng Huang was born in Anhui, China, in 1999. He received the B.S. degree in electrical engineering from Anhui University of Technology, Ma'anshan, China, in 2021, where he is currently pursuing the M.S. degree in electrical engineering. His research interests include large signal stability analysis of distributed DC microgrid cluster systems, and nonlinear control. He published a conference paper and has 1 patent pending.

Qianjin Zhang received his Ph.D. degree in power electronics from Chongqing University, Chongqing, China, in 2020.

He was a Visiting Scholar in the University of Exeter, Penryn, U.K., from May 2018 to May 2019. He is presently a Lecture with Anhui University of Technology, Anhui, China. His research interests include PV power generation, the modeling, control, and stability analysis of power electronics system.

Wei Fang was born in Anhui Province, China, in 1977. He received the B.S. degree from Anhui University of Technology, Anhui, China, in 1998, and M.S. and Ph.D. degrees from Nanjing University of Aeronautics and Astronautics, Nanjing, China, in 2004 and 2008, respectively. He has been with Anhui University of Technology, since 2008 and is currently a professor in the School of Electrical and Information Engineering, Anhui University of Technology. He was a visiting scholar at Queen's University, Kinston, Ontario, Canada, from Sept. 2010 to Feb. 2011. His research interests are in the areas of switching power converters, and renewable energy.

Xiaodong Liu was born in Jilin, China, in 1971. He received the Ph.D. degree in electric machines and electric apparatus from Zhejiang University, Hangzhou, China, in 1999. Since 2003, he has been with the School of Electrical and Information Engineering, Anhui University of Technology, Ma'anshan, China, where he is now a full professor. He was a visiting scholar at Queen's University, Kinston, Ontario, Canada, from July 2007 to Oct. 2007. His major fields of interest include the dc-dc switching converter, power factor correction techniques, and motor design and driving control.